AAPS PharmSciTech (2023) 24:91
https://doi.org/10.1208/s12249-023-02552-5

RESEARCH ARTICLE

Assessment of Tribo-charging and Continuous Feeding Performance of Direct Compression Grades of Isomalt and Mannitol Powders

Michela Beretta[1,2] · Julia Kruisz[1] · Theresa R. Hörmann-Kincses[1] · Viktoria Magosi[1] · Meishan Guo[3] · Majid Naderi[3] · Sarah Heupl[4] · Johann Kastner[4] · Martin Spoerk[1] · Amrit Paudel[1,2]

Received: 14 December 2022 / Accepted: 6 March 2023 / Published online: 28 March 2023

Abstract

Tribo-charging is often a root cause of mass flow deviations and powder adhesion during continuous feeding. Thus, it may critically impact product quality. In this study, we characterized the volumetric (split- and pre-blend) feeding behavior and process-induced charge of two direct compression grades of polyols, galenIQ™ 721 (G721) for isomalt and PEARLITOL® 200SD (P200SD) for mannitol, under different processing conditions. The feeding mass flow range and variability, hopper end fill level, and powder adhesion were profiled. The feeding-induced tribo-charging was measured using a Faraday cup. Both materials were comprehensively characterized for relevant powder properties, and their tribo-charging was investigated for its dependence on particle size and relative humidity. During split-feeding experiments, G721 showed a comparable feeding performance to P200SD with lower tribo-charging and adhesion to the screw outlet of the feeder. Depending on the processing condition, the charge density of G721 ranged from -0.01 up to -0.39 nC/g, and for P200SD from -3.19 up to -5.99 nC/g. Rather than differences in the particle size distribution of the two materials, their distinct surface and structural characteristics were found as the main factors affecting their tribo-charging. The good feeding performance of both polyol grades was also maintained during pre-blend feeding, where reduced tribo-charging and adhesion propensity was observed for P200SD (decreasing from -5.27 to -0.17 nC/g under the same feeding settings). Here, it is proposed that the mitigation of tribo-charging occurs due to a particle size-driven mechanism.

Keywords continuous manufacturing · isomalt · mannitol · tribo-charging · twin-screw powder feeding

Introduction

The mono- and disaccharide alcohols (polyols) are excipients in pharmaceutical tablet formulations [1, 2]. The polyols are of a non-animal origin and bear the advantage of being non-cariogenic with low hygroscopicity, pleasant taste, and reduced caloric content [1, 3]. Polyols are widely acceptable by patients (*e.g.*, diabetic and lactose-intolerant patients [4]), and the absence of a carbonyl group makes them chemically stable (*e.g.*, do not undergo Maillard reactions with amine drug's functional groups [5]).

Within the polyols, mannitol has gained prominence as pharmaceutical excipient in solid dosage forms [2]. Another polyol, isomalt, has been mainly used as food ingredient and was introduced as pharmaceutical excipient in 2005 [3]. Compared to mannitol, which has been already used as excipient in formulations for continuous direct compression (CDC) [6–8], to the best of the authors' knowledge, there is currently no report of the use of isomalt as filler-binder for CDC applications. However, beneficial properties of the direct compression (DC) isomalt grades as low adhesion tendency [1] and tribo-charging propensity [9], low sensitivity to lubrication [3], and good compressibility [1, 3, 10, 11] have been highlighted together with good mechanical properties [12] and solubility characteristics [13]. These properties may become critical for continuous manufacturing (CM) processes, where

✉ Amrit Paudel
amrit.paudel@rcpe.at

1 Research Center Pharmaceutical Engineering GmbH, Inffeldgasse 13/II, 8010 Graz, Austria

2 Institute of Process and Particle Engineering, Graz University of Technology, 8010 Graz, Austria

3 Surface Measurement Systems Ltd, Wembley HA0 4PE, UK

4 University of Applied Sciences Upper Austria, Campus Wels, 4600 Wels, Austria

materials need to be processed over a long period of time without interruptions. Contrary to batch processes, during CM, particle contact interactions are facilitated. Thus, phenomena such as the surface exchange of charged species (*i.e.*, electrons, ions, material fragments, or combinations thereof), known as tribo-charging, can develop more easily [14]. Powder tribo-charging has been suggested as a potential root cause for inaccuracy and inconsistency of the feeding process [15–17], the (fore)most critical step inherent to all CM processes [18]. Therefore, there is a growing interest in characterizing the tribo-charging tendency of powders as a critical material attribute for feeding performance [19–21]. Powders adhering to the feeder surfaces undergo higher tribo-charging, resulting in stagnation in the hopper, reduction of the screw free volume, bearding effects at the screw outlet (*i.e.*, adhesion to the screw outlet), and alteration to the powder trajectory during free-fall motion [22] and hopper refilling [23]. This can block feeder refilling leading to poor accuracy and consistency of the dosed mass, which may propagate throughout the process and lead to products with varying content of active pharmaceutical ingredient(s) (APIs). The common practice of grounding processing equipment has been in fact demonstrated to be less efficient than generally thought in reducing electrostatic charging [24, 25]. To mitigate such risk to product quality, powders that are challenging to feed as raw materials (*i.e.*, split-feeding) are typically mixed with other components to improve their feeding performance (*i.e.*, pre-blend feeding) [18, 20]. A trial-and-error approach is often used in those cases, as powder tribo-charging has still not been entirely understood. Factors affecting the tribo-charging propensity can be related to material (*e.g.*, work function, surface chemistry, crystallinity, particle size and morphology, moisture content, surface roughness, mechanical properties), formulation (*e.g.*, blend type, API(s) concentration), and process conditions (*e.g.*, equipment surface, process parameters, environmental conditions) [26]. There are several complex factor interactions that occur during pharmaceutical manufacturing (*e.g.*, materials differ for more than one parameter, undergo different handling history, are subjected to distinct contact types). Therefore, concerns have been raised regarding the comparability of the results among different laboratories as well as the transferability of the findings during process scale-up [27]. These two aspects were addressed in our previous work where we attempted to (i) identify the principal material attributes affecting the tribo-charging of common pharmaceutical powders for CM under standardized conditions and (ii) establish a link between the charge results of a lab-scale measurement device and the ones developing during processing in a small-scale twin-screw feeder [22]. We also investigated the effect of relative humidity (RH) on the bulk powder behavior and tribo-charging, which was found to depend on material-water interactions [28].

In this study, using DC grades of mannitol and isomalt, we extended our feeding investigation beyond our previous work [22], including a different set of process conditions (*i.e.*, shear and normal stresses) and feeding strategies (*i.e.*, split- and pre-blend feeding) in a pilot-scale feeder. To explain the resulting observations, the powders were additionally characterized for relevant powder properties, and their tribo-charging behavior was investigated for its dependency on particle size and RH.

Materials and Methods

Materials

The agglomerated isomalt galenIQ™ 721 (G721, BENEO-Palatinit GmbH, Germany) and the spray-dried mannitol grade PEARLITOL® 200SD (P200SD, Roquette, France) were investigated in the present study. G721 is a disaccharide alcohol consisting of a 6-O-α-D-glucopyranosyl-D-sorbitol/1-O-α-D-glucopyranosyl-D-mannitol dihydrate (GPS/GPM) ratio of 3:1 [3]. P200SD is a mixture of α- and β-mannitol polymorphs [29]. For the preparation of the respective binary blends, an E124 colored food dye (tracer, Wurth Essenzenfabrik GmbH, Austria) was sieved below 45 µm to resemble a model API.

Material Conditioning

Prior to the experiments, if not stated otherwise, the powders were stored at 43% RH for 48 h to minimize the impact of possible variations in environmental conditions on the feeding and material characterization results. For that, materials were placed either in RH-controlled labs (prior to feeding runs) or in sealed desiccators (prior to material characterization). To study powder tribo-electrification as a function of RH, the powders were stored inside desiccators supplemented with saturated salt solutions of potassium acetate (23% RH), potassium carbonate (43% RH), and potassium iodide (69% RH) [30]. All salts were purchased from Sigma-Aldrich (Germany).

Twin-Screw Feeding Experiments

Feeding experiments were performed using both split-feeding and pre-blend feeding to evaluate the powder feeding performance and characterize the respective feeding-induced charge.

Experimental Set-up

The experimental set-up (Fig. 1) consists of a pilot-scale K-CL-KT20 feeder (Coperion K-Tron GmbH, Germany), two cameras, a reference catch-scale, and a Faraday cup. The feeder was equipped with coarse concave screws and was monitored by two cameras (C920 full HD cameras, Logitech, Switzerland). The reference catch-scale type SW 1000/1000-FS (Wipotec, Germany) was used for an independent determination of the mass flow, and the Faraday cup of the GranuCharge™ device (GranuTools, Belgium) was used for in-process charge measurements.

Feeding Runs and Measurement of Process-Induced Charge

Contrary to the gravimetric feeding operation commonly applied in CM, all feeding runs were carried out in volumetric mode (*i.e.*, fixed screw speed) to expose the materials to the same level of shear and to evaluate the material-feeder interaction independently from the feeder controller [31].

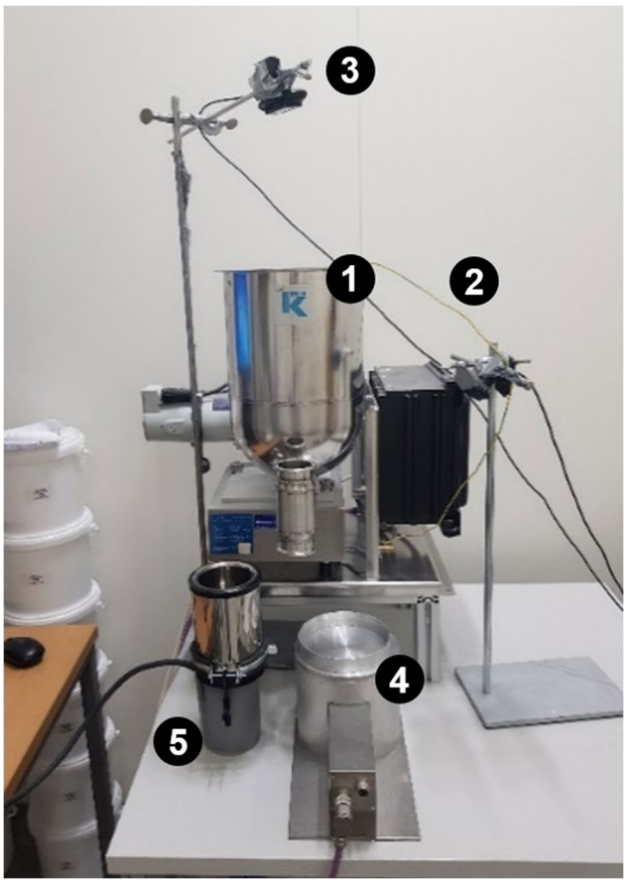

Fig. 1 Experimental set-up for feeding experiments: K-CL-KT20 feeder (1) with a grounding cable (2), two cameras (3), reference catch-scale (4), and Faraday cup (5)

For the split-feeding runs, two different hopper fill levels (*i.e.*, hopper initially filled with powder up to 100% and 40% of its total volume) and screw speeds (*i.e.*, 20 and 50% of the maximum screw speed of 154 rpm) were selected to evaluate the impact of different powder compression states and shear rates. The pre-blend feeding runs were carried out at fixed process parameters of 100% initial hopper fill level and 50% screw speed.

The process-induced charge measurements were performed according to the procedure described previously [22]. The measurements were made at 3, 6, and 9 min from the process start by collecting approx. 10 g of the powder being fed by the feeder in the Faraday cup. Feeding runs were performed in duplicate at 23 ± 1 °C/42 ± 2% RH. The feeding experiments will be identified throughout this manuscript using the following notation: split-/pre-blend feeding_initial fill level_screw speed (S/PB_FL_SS).

Evaluation of Feeding Performance

The gain-in-weight data collected from the reference catch-scale were evaluated to obtain information on the feeding performance. As indicators for the feeding process performance, the following metrics were selected [31–33]:

i) The average mass flow at 20% and 50% screw speeds over the first 2 min (MF_{2min}) of the feeding run as indication of the screw conveying capacity
ii) The feed factor (FF) as indication of maximum feed capacity
iii) The relative deviation to the mean (RDM) of the mass flow throughout the feeding as a measure of mass flow consistency upon bulk density changes during hopper emptying
iv) The hopper end fill level (EFL) as indication of the ability to empty the hopper (risk of flow stagnation)

More details on the feeding set-up, experimental execution, and selected feeding metrics can be found in the supplementary material (Figure A1 and descriptions).

Material Characterization

Material Sieving and Small-Scale Blending

If not stated otherwise, material characterization was performed on the powders with an untreated particle size distribution. Sieved fractions of G721 (a fine fraction below 100 µm, an intermediate fraction in the range of 100–250 µm, and a coarse fraction above 250 µm) were used to investigate its tribo-charging dependence on particle size and to obtain a sample with a comparable particle size to P200SD. To investigate the impact of different additives (*i.e.*, same-material

and tracer fines) on the acquired charge, G721 and P200SD were sieved through a 45-µm mesh, and small-scale powder blends (10 g) comprising raw materials and 1 wt% of their respective sieved fines (below 45 µm) were prepared.

Particle and Bulk Characterization

The samples were investigated for the particle size and shape distribution, inner structure, specific surface area (SSA) and pore distribution, water content, surface energy, density, and flow characteristics.

The particle size and shape distribution of the samples, indicated as volume-based particle size (D_{v10}, D_{v50} and D_{v90}), span, and aspect ratio (AR), were determined using the QICPIC/L dynamic image analysis apparatus (Sympatec GmbH, Germany).

The inner structure of the particles was analyzed using X-ray micro-computed tomography (µ-CT) [34] on the RX Easytom 160 (RX Solutions, France). The SSA and the pore distribution in the size range of 1.7–300 nm were determined from nitrogen gas adsorption measurements using a TriStar II 3020 system (Micromeritics, USA). The SSA was determined applying the Brunauer–Emmett–Teller (BET) theory, whereas the pore size distribution was determined using the Barrett-Joyner-Halenda (BJH) method [35]. In addition, mercury intrusion porosimetry (MIP) was performed on a POREMASTER® 60GT (Quantachrome Instruments, Germany) to evaluate the meso- and macro-pore size distribution (in the range of 6 nm to 230 µm) applying the Washburn equation [36].

The water content of the powders was measured via Coulometric Karl Fischer titration, using a TitroLine 7500 KF trace (SI Analytics, Germany).

The surface energy of the materials ($\gamma_S{}^T$) was characterized on an iGC-Surface Energy Analyzer (iGC-SEA, Surface Measurement Systems Ltd., UK). The dispersive component ($\gamma_S{}^D$) was determined based on the Dorris and Gray method [37]. The acid–base component ($\gamma_S{}^{AB}$) was instead estimated according to the van Oss approach [38] and subdivided into its acid ($\gamma_S{}^+$) and base ($\gamma_S{}^-$) parameters. From the surface energy data, the work of cohesion (W_C) and the work of adhesion (W_A) were calculated according to [39], assuming the surface energy parameters of a 316L type of stainless steel with a 2B surface finishing from literature [40].

The bulk (BD) and tapped (TD) density of the powders were determined using the cylinder method [41] on a Pharma Test PT-TD200 (Pharma Test, Germany), and the derived Hausner ratio (HR) and Carr index (CI) were selected as flowability descriptors.

Tribo-charging

The tribo-charging propensity of the raw materials as a function of their particle size and environmental conditions was assessed using the GranuCharge™ device. The initial charge (Q_0) was determined by pouring approx. 10 g of powder in the Faraday cup. After the Q_0 determination, the powder was transferred in a stainless steel vibratory chute, which conveyed the powder into a grounded stainless steel V-tube. Following particle–particle, particle–surface frictional contacts, and impact with the V-tube [9], the charged material was then collected into the Faraday cup to determine the charge after contact (Q_1). The charge density (q) was calculated by dividing the measured charge (Q) by the sample weight and the acquired charge calculated as $q_1 - q_0$.

More details on all methods and respective calculations can be found in the supplementary material.

Results

Analysis of the Split-Feeding and Pre-blend Feeding Performance

Examples of the mass flow plots obtained during feeding experiments are shown in the supplementary material (Figure A2), whereas the estimated feeding performance metrics is reported in Table I.

Overall, both G721 and P200SD showed good feeding performance (high MF and FF, low RDM and EFL) across all the process conditions and feeding strategies tested. In all cases, a slightly higher mass flow was observed for P200SD. Likewise, a higher conveying capacity at full speed (FF) was calculated for P200SD at both fill levels. A generally lower RDM was instead observed for G721 (except for the PB_100_50 run), reflecting its stable MF profile throughout the entire fill level range. Moreover, both powders were able to completely empty the hopper resulting in a low residual mass in the hopper at the end of each feeding experiment (EFL < 4% in all cases).

To qualitatively evaluate the extent of powder adhesion to the feeder surfaces, pictures were taken at the end of each feeding run and reported in Fig. 2.

A minimal extent of adhesion was observed for G721 powder at all conditions on the screws (Fig. 2a and d) and at the screw outlet (Fig. 2b and e). Instead, a higher adhesion to the feeder outlet (Fig. 2h) and at the screw tip (Fig. 2g) was evident for P200SD during split-feeding runs and became more pronounced at higher screw speeds (Fig. 2j and k). Similar findings have been observed, to a higher extent, by Allenspach *et al.* when feeding hydroxypropyl methylcellulose (HPMC) K4M powder and have been associated to an electrostatic powder build-up [23].

Results of the magnitude of process-induced charge measured during split-feeding and pre-blend feeding experiments are reported in Fig. 3.

Table I Overview of the Feeding Performance Metrics Computed for Each Feeding Run (Identified by Split-/Pre-blend Feeding_Initial Fill Level_Screw Speed): MF_{2min} mass flow, *FF* feed factor, *RDM* Relative Deviation to the Mean, and *EFL* end fill level ($n=2$; Mean ± Range)

Material	Feeding run ID (S/PB_IFL_SS)	MF_{2min} (kg/h)	FF (kg/h)	RDM (%)	EFL (%)
G721	S_100_20	3.56 ± 0.24	17.82 ± 1.21	2.04 ± 0.15	3.94 ± 1.32
	S_40_20	2.97 ± 0.05	14.84 ± 0.26	1.19 ± 0.13	2.68 ± 0.07
	S_100_50	8.81 ± 0.25	17.62 ± 0.50	2.14 ± 0.13	2.61 ± 0.22
	S_40_50	7.45 ± 0.02	14.90 ± 0.05	1.34 ± 0.00	2.87 ± 0.07
	PB_100_50	9.52 ± 1.22	19.05 ± 2.45	3.86 ± 2.01	3.50 ± 0.01
P200SD	S_100_20	4.35 ± 0.09	21.73 ± 0.45	2.76 ± 1.14	1.51 ± 0.44
	S_40_20	3.95 ± 0.05	19.73 ± 0.25	5.53 ± 1.26	2.35 ± 0.35
	S_100_50	10.43 ± 0.05	20.86 ± 0.09	4.95 ± 0.50	3.20 ± 0.63
	S_40_50	9.64 ± 0.01	19.27 ± 0.03	4.37 ± 0.36	2.81 ± 0.67
	PB_100_50	10.34 ± 0.05	20.68 ± 0.11	2.01 ± 0.06	2.13 ± 0.13

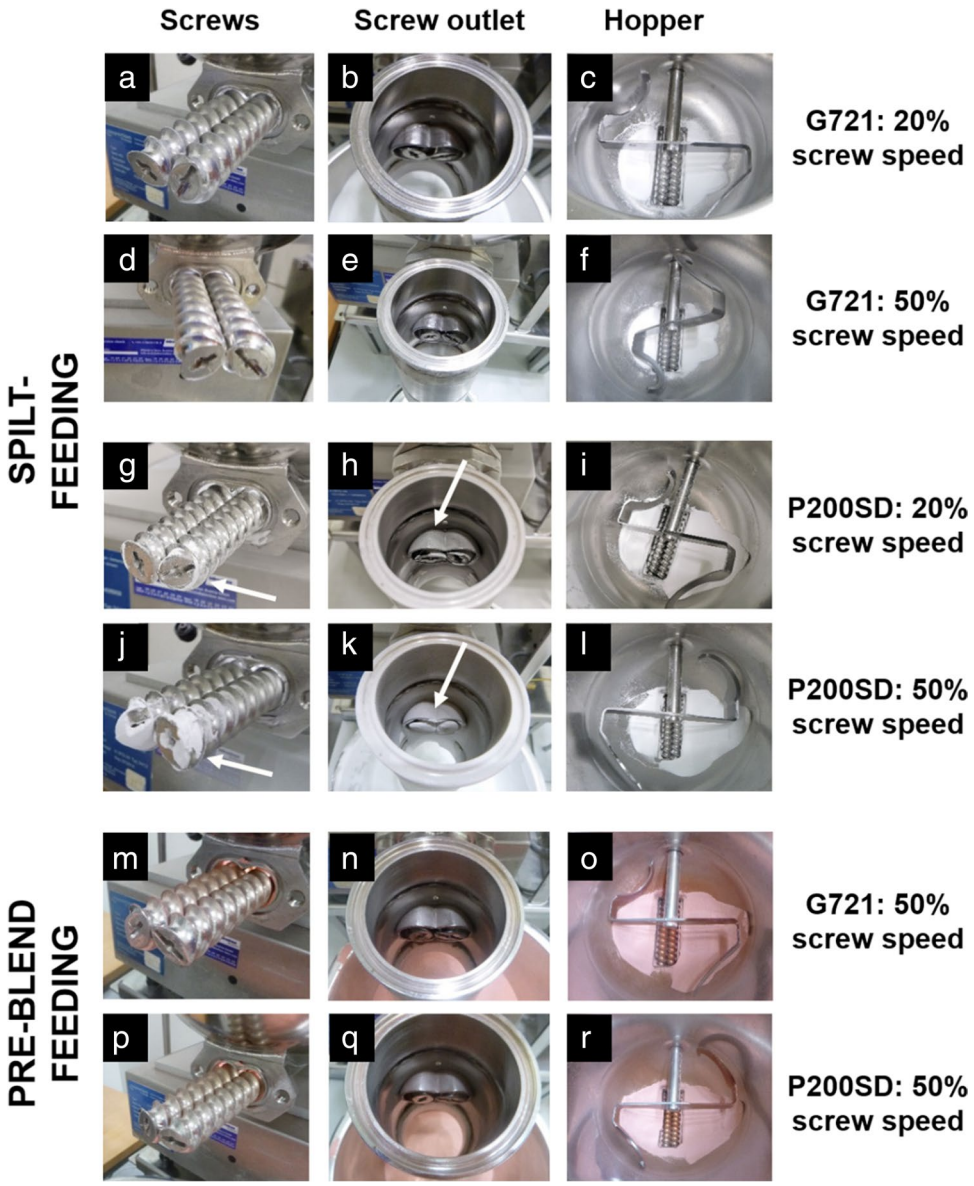

Fig. 2 Pictures of feeder elements showing the extent of powder adhesion to the screws, screw outlet, and residual mass in the hopper for split-feeding runs (performed at 100% initial fill level with G721 (**a-f**) and P200SD (**g-l**) at 20% and 50% screw speeds) and pre-blend feeding runs (performed at 100% initial fill level and 50% screw speeds with pre-blends comprising G721 (**m-o**) and P200SD (**p-r**) powders with 1 wt% of sieved tracer, respectively). Arrows indicating powder adhesion

An extremely low charge density was observed for G721 at all consolidation states and shear rates when fed as a raw material. A slight, yet significant ($p < 0.05$), increase in charge density was only observed for the run at the highest fill level and screw speed (S_100_50). Likewise, G721 powder was found to charge to a minimal extent during pre-blend feeding showing comparable values to the split-feeding runs.

Compared to G721, P200SD was found to undergo significantly higher tribo-charging during split-feeding, and its charge was only slightly reduced when fed at 100% hopper fill level and 20% screw speed. Interestingly, the relatively high charge density observed during split-feeding experiments was drastically reduced when adding 1 wt% tracer and reached even a lower charge level compared to G721.

Powder Characterization

Determination of Particle Size and Shape

The particle size distribution (PSD) and shape of the starting materials and respective sieved fractions are reported in Table II. Differences in the PSD of the starting materials were observed with G721 showing a broader distribution compared to the P200SD powder. For both materials, a high AR was measured indicating a rather spherical particle shape, which is in agreement with literature [1, 29]. With regard to the sieved powders, the intermediate size fraction of G721 (100 µm < G721 < 250 µm) was found to have a comparable PSD to the starting P200SD. Likewise, a similar PSD was obtained for the sieved colored tracer and the fine fractions of G721 and P200SD sieved below 45 µm.

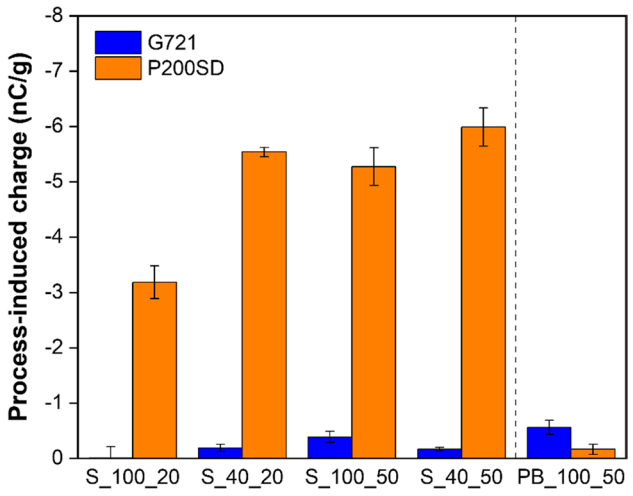

Fig. 3 Measured process-induced charge following split-feeding and pre-blend feeding identified as split-/pre-blend feeding_initial fill level_screw speed ($n = 6$; Mean ± SD)

Characterization of the Inner Particle Structure

The inner structure of the starting materials is reported in Fig. 4. The two samples revealed different structures, with G721 showing a dense inner structure and P200SD a porous one. The inner structure of P200SD presented a high concentration of internal cavities with different dimensions (both small and large pores), characteristic of spray-dried powders under given process parameters [42].

Evaluation of the Specific Surface Area and Pore Size Distribution

The SSA and pore size distribution of the investigated powders, measured via nitrogen gas adsorption, are reported in Table III. The SSA of P200SD was approx. twice as large as that of G721. Moreover, P200SD showed the presence of larger pores in agreement with the structure identified by µ-CT. This observation has been further confirmed from the MIP curves reported in Fig. 5. The intrusion curve of P200SD showed a first intrusion step in the pore size range of approx. 100–20 µm (characteristic of inter-particle voids filling) and a second, less pronounced step, in the range of approx. 5–0.1 µm (corresponding to the actual pore filling). In contrast, only one broad intrusion step (in the range of approx. 200–1 µm) could be observed for G721. In this case, the transition to an eventual pore filling step is smooth and uniform.

Table II Overview of the Relevant Particle Size Distribution (PSD) Parameters and Aspect Ratios (AR) of the Investigated Starting Materials and Respective Sieved Fractions ($n = 3$; Mean ± SD)

Sample	Dv_{10} (µm)	Dv_{50} (µm)	Dv_{90} (µm)	Span (-)	AR_{50} (-)
G721	110.92 ± 4.99	254.44 ± 9.96	391.22 38.07	1.10 ± 0.12	0.87 ± 0.01
P200SD	107.85 ± 1.69	164.07 ± 2.93	227.76 ± 4.82	0.73 ± 0.02	0.86 ± 0.01
G721 (< 100 µm)	39.97 ± 0.35	73.85 ± 0.32	107.20 ± 0.26	0.91 ± 0.01	0.80 ± 0.00
G721 (100–250 µm)	80.98 ± 0.80	157.98 ± 0.98	230.99 ± 1.11	0.95 ± 0.01	0.84 ± 0.00
G721 (> 250 µm)	165.01 ± 0.66	297.63 ± 3.63	454.05 ± 15.83	0.97 ± 0.04	0.82 ± 0.00
G721 (< 45 µm)	17.43 ± 0.19	37.72 ± 0.30	58.08 ± 1.73	1.08 ± 0.04	0.75 ± 0.00
P200SD (< 45 µm)	12.43 ± 0.22	36.12 ± 0.84	61.07 ± 2.60	1.35 ± 0.05	0.75 ± 0.00
Tracer (< 45 µm)	4.41 ± 0.05	26.38 ± 3.28	48.67 ± 0.21	1.70 ± 0.22	0.79 ± 0.00

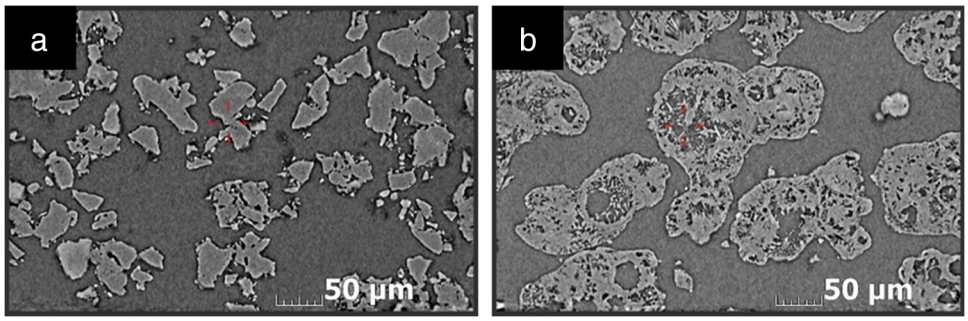

Fig. 4 X-ray micro-computed tomography (µ-CT) images of G721 (**a**) and P200SD (**b**) powders

Table III Overview of the Specific Surface Area (SSA) and Barrett-Joyner-Halenda (BJH) Pore Size and Volume of the Investigated Starting Materials ($n=3$; Mean ± SD)

Sample	*SSA (m^2/g)*	*BJH pore size (nm)*	*BJH pore volume (mm^3/g)*
G721	0.44 ± 0.01	12.45 ± 1.54	0.92 ± 0.06
P200SD	1.14 ± 0.02	14.68 ± 1.99	4.30 ± 0.57

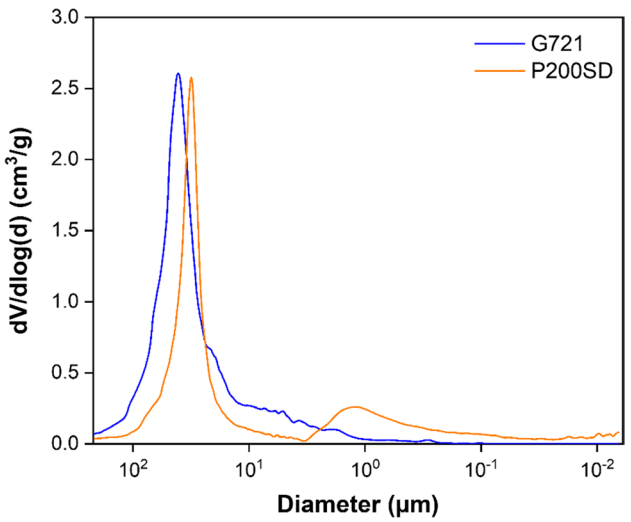

Fig. 5 Mercury intrusion porosimetry (MIP) profiles for the starting G721 and P200SD powders

Determination of the Water Content

Results of the water content measurements, performed after storing the starting materials at three RH levels, are reported in Table IV. Both powders showed only a slight increase in water content when stored at 69% RH. The total water content of G721 (approx. 3 wt%), measured via Karl Fischer titration, was significantly higher compared to that of P200SD (approx. 0.1 wt%). However, G721 is a dihydrate crystalline material containing two water molecules per GPM component. Based on dynamic vapor sorption (DVS) analysis (data not shown), 2.3 wt% of the total water content

Table IV Water Content Determined for the Starting Materials at 23, 43, and 69% RH After 48 h of Storage ($n=2$; Mean ± Range)

Sample	*Water content (wt%)*		
	23% RH	*43% RH*	*69% RH*
G721	2.97 ± 0.02	3.04 ± 0.02	3.13 ± 0.01
P200SD	0.09 ± 0.00	0.10 ± 0.00	0.15 ± 0.01

of G721 consists of bound water (crystal water), and the residual 0.7–0.8 wt% is unbound (surface) water. In terms of unbound water, a higher fraction of water molecules is expected for the G721 particles.

Characterization of the Surface Energy

The surface energy profiles of the starting G721 and P200SD powders in the surface coverage range of 0.005–0.2 are reported in Fig. 6. An overview of the respective numerical values at an intermediate surface coverage of 0.1 is reported in Table V together with the calculated W_c and W_A to stainless steel.

From the surface energy profiles (Fig. 6), it is evident that P200SD is energetically more heterogeneous than G721, meaning that its surface energy varies as a function of the surface coverage due to the presence of surface sites of different energy levels. Both powders were found to possess basic (electron-donor) characteristics ($\gamma_s^+/\gamma_s^- < 1$), more pronounced in the case of P200SD. The dominant contribution to the total surface energy was represented by their dispersive component for both powders. However, G721 showed a higher W_A compared to W_C, whereas opposite findings were observed for P200SD. This indicates that, compared to P200SD, G721 will more easily spread over the stainless steel surface leading to higher particle–surface interactions [39].

Determination of Bulk and Tapped Density and Derived Flow Descriptors

The densities and flow characteristics of the powders are reported in Table VI. Compared to G721 powder, a higher

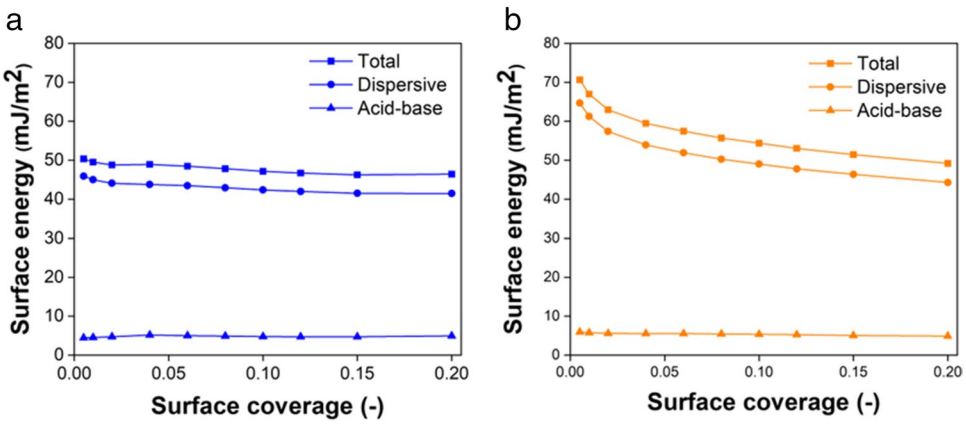

Fig. 6 Surface energy profiles obtained for G721 (**a**) and P200SD (**b**) in the surface coverage range of 0.005–0.2

Table V Dispersive (γ_s^D), Acid (γ_s^+), and Base (γ_s^-) Components of the Surface Energy (γ_s^T) Calculated at a Surface Coverage of 0.1 and the Respective Work of Cohesion (W_C) and Work of Adhesion (W_A) to Stainless Steel

Sample	$\gamma_s^D(mJ/m^2)$	$\gamma_s^+(mJ/m^2)$	$\gamma_s^-(mJ/m^2)$	$\gamma_s^T(mJ/m^2)$	$W_C(mJ/m^2)$	$W_A(mJ/m^2)$
G721	42.35	1.99	2.87	47.12	94.24	99.50
P200SD	49.02	1.93	3.74	54.38	108.77	106.49

BD and TD as well as better flowability were measured for P200SD. According to the flowability classification of Carr [43], the HR and CI values determined for G721 (in the range of 1.26–1.34 and 21–25, respectively) suggest a "passable" flow character, whereas the ones obtained for P200SD (in the HR range of 1.12–1.18 and CI range of 11–15) indicate a "good" flow character. Generally, the HR and CI measured for the G721 powder are slightly higher than the values reported in literature [3], whereas the ones of P200SD are in good agreement [29, 44].

Evaluation of Powder Tribo-charging on the GranuCharge™ Device

Tribo-Charging Dependence on Particle Size

To verify whether the difference in the tribo-charging of the two powders was driven by their distinct PSD [45, 46], the sieved size fractions of G721 were compared to P200SD in Fig. 7a. When benchmarking G721 and P200SD powders with comparable PSD (100 µm < G721 < 250 µm), P200SD was still found to charge to a higher extent suggesting the contribution of other factors to its tribo-electrification. Compared to the raw G721 powder, all its sieved fractions resulted in a reduced charging propensity, and interestingly, the lowest charge density value was obtained for the smallest particle size (< 100 µm). This is in agreement with previous findings reporting higher charge magnitudes for materials with a broader PSD [47]. When adding 1 wt% of fines to the starting materials, the tribo-charging propensity of P200SD was reduced, whereas for G721, this had a negligible impact.

Table VI Bulk (BD) and Tapped Density (TD) of the Investigated Powders and Derived Flow Descriptors such as Hausner Ratio (HR) and Compressibility Index (CI) ($n = 3$; Mean ± SD)

Sample	*BD (g/ml)*	*TD (g/ml)*	*HR (-)*	*CI (%)*
G721	0.41 ± 0.02	0.54 ± 0.00	1.33 ± 0.06	24.80 ± 3.49
P200SD	0.53 ± 0.01	0.62 ± 0.00	1.18 ± 0.01	14.93 ± 0.61

Tribo-Charging Dependence on Relative Humidity

The tribo-charging propensity of the powders was evaluated at a relatively dry (23% RH), intermediate (43% RH), and a more wet condition (69% RH). The tribo-charging results are reported in Fig. 7b. A higher charge density was observed for P200SD at all RH levels, which is in agreement with literature [9]. For both powders, a similar charging trend with RH was observed, where the charge density increased from 23 to 43% RH and decreased at 69% RH (without reaching the minimum charge level obtained at 23% RH).

Discussion

Effect of Material Attributes on Feeding Performance

With the strides to continuous pharmaceutical manufacturing, the importance in the characterization of the feeding

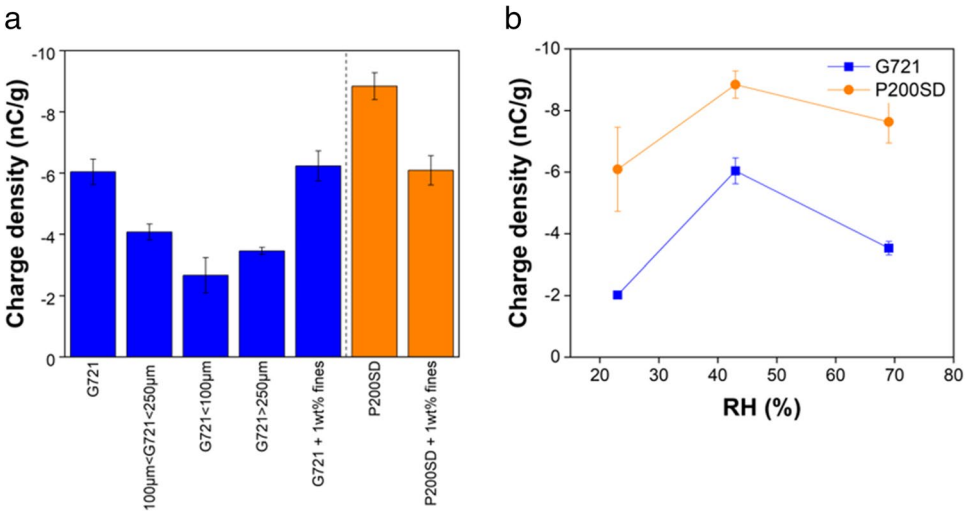

Fig. 7 Dependence of the charge density on the particle size distribution (**a**) and relative humidity (**b**) ($n = 6$; Mean ± SD)

performance of powders has raised as it is crucial for the long-term stability of the entire CM process. Many studies have been conducted under process-relevant gravimetric feeding mode. To gain understanding of the material-feeder interaction, volumetric feeding studies have also been performed [19, 21, 31, 41]. The volumetric feeding performance of the two polyols grades investigated in this study was found to be consistent across all the feeding strategies and process conditions tested and resulted in relatively high levels of mass flow. Based on the estimation of the mass flow at full speed (FF), the mass flow rates in typical continuous pilot-scale operations (*e.g.*, 10–15 kg/h) could be met for both powders with the given feeder configuration (Table I). The feeding process was stable throughout its entire duration (*i.e.*, low RDM), and a slight decrease in mass flow was observed for P200SD at hopper fill levels below 40%. Such effect can be erased during a continuous gravimetric feeding operation (compensated by feeder controller) and by selecting a suitable refilling strategy.

Overall, a slightly higher mass flow was obtained for P200SD associated to the higher bulk density and flowability measured for this material, which is expected to result in a more efficient degree of screw filling. Bearding effects were visible during split-feeding runs for P200SD, and a higher extent of powder adhesion to the screw outlet and screw tip was observed at higher screw speeds. Such adhesion propensity may worsen during longer processing, posing risks for mass flow deviations (*e.g.*, by a sudden dislodgment of the powder accumulated at the feeder outlet) [23]. The absence of bearding effects and a minimal tendency to adhere to the feeder surfaces were instead obtained for G721. Such differences in the adhesion tendency [1] were found to correlate to the process-induced charge. Tribo-charging has been a root cause for the adhesion propensities of powders [23, 48]. However, adhesion forces consist of electrostatic and non-electrostatic components (van der Waals forces) acting at different length scales [49]. The higher extent of charge generated during the feeding process for P200SD (Fig. 3) may be responsible for bringing the powder into contact with the feeder surface. Once the separation distances are reduced in the order of tens of nanometer, short-range van der Waals interactions prevail and make the powder adhere to the surface [50]. This is supported by the higher dispersive component of the surface energy (representing van der Waals interactions) measured for P200SD (Fig. 6).

Contrary to G721, for which a minimal charge density and powder adhesion was overall observed, the addition of only 1 wt% of fine particles of colored tracer in P200SD resulted in a significant charge mitigation and reduction in powder adhesion. Hypotheses to explain such behavior are formulated in the next section.

Mechanisms Behind Powder Tribo-charging

Results of this study are in agreement with our previous findings [22], attesting the suitability of a small-scale charge analysis to evaluate trends in powder tribo-charging following feeding operations. The tribo-charging measured on the GranuCharge™ at similar environmental conditions as the process-induced charge determinations revealed the same lower tribo-charging and adhesion propensity of G721 compared to P200SD. Also, differences were observed in terms of charge magnitude between the two experimental set-ups. The lower charge density observed during feeding may be associated to the higher number of particle–particle contacts in relation to the particle–wall contacts or to prolonged contacts with the grounded feeder surface.

Tribo-charging is a multifactorial phenomenon, known to be affected by differences in powder properties, process, and environmental conditions [26]. Therefore, the process-induced charge of both G721 and P200SD was characterized under different process parameters (shear and compression),

and a separate investigation on the effect of distinct RH levels on tribo-charging was performed. In both cases, despite strong differences in terms of charge magnitude, similar charging trends were observed for the investigated materials. The process-induced charge was generally found to be consistent across the range of process conditions investigated (with exception of the run with P200SD at 100% initial fill level and 20% screw speed). Additionally, a similar trend of increasing charge from 23 to 43% RH followed by a charge decrease from 43 to 69% RH was observed. This can be explained by the presence of water molecules that can facilitate charge transfer via conductive bridges at lower RH [51] and lead to charge reduction by increasing surface conductivity at higher RH [51]. Those results suggest that the strong difference in charge magnitude observed between the powders is not affected by process and environmental conditions but predominantly driven by their distinct powder characteristics. When analyzing the powder tribo-charging dependence on particle size, the G721 fraction with a comparable PSD to P200SD showed a lower charge density. Thus, the minimal charging propensity of G721 cannot be explained by its characteristic particle size suggesting the contribution of other powder properties.

A porous structure with a higher surface heterogeneity was revealed for the spray-dried P200SD [42]. The tribo-charging behavior of powders can be significantly affected by surface modifications and can be correlated to changes in surface energy [39]. The presence of sites with different energy levels would lead to localized accumulations of charge and result in an uneven charge distribution on the surface [52]. The comparatively lower amount of surface water present on the P200SD particles may not be enough to guarantee an efficient charge relaxation process or may even help promote tribo-electrification [28, 53]. This effect may play a major role when the charging mechanism relies on the exchange of other charge species than electrons. The electron donor characteristics of the powders observed in the surface energy analysis were not reflected in the negative polarity of the measured charge, which may imply the transfer of other charge species. In contrast to P200SD, the denser surface of G721 particles may facilitate a homogeneous distribution of charge and the formation of a uniform distribution of water molecules. It can be therefore hypothesized that the overall charge present on the surface of the G721 particles is dissipated more rapidly due to the enhanced particle conductivity associated with the presence of the water layer [28, 53] and the enhanced contact with the stainless steel surface for charge neutralization (the higher adhesion/cohesion energy ratio shown in Table V) [39].

The effect of different mechanical properties of the two powders (i.e., G721 undergoing a brittle-plastic whereas P200SD a brittle deformation) [12] on the mode of contact and thus their overall tribo-electrification [54, 55] cannot be ruled out.

As a potential mitigation strategy, the addition of only 1 wt% of tracer fines resulted in a reduction of the tribo-charging propensity of the P200SD powder. In contrast, this had a negligible effect on the minimal charge density obtained for G721. This effect seems to be particle size driven rather than a chemistry-mediated, as when adding 1 wt% of the same-material fines, the same tribo-charging trend could be observed. Most likely, the charge mitigation results from the difference in charge polarity obtained during same-material tribo-charging for coarse and fine fractions (typically carrying a positive and negative charge, respectively) [47, 56, 57].

Practical Implications and Limitations

The first step towards CM process design is the reliability of the feeding system and its impact on downstream steps. Despite this study being restricted to the specific grades of polyols, the insights on their adhesion propensities and the strategies for their potential mitigation are expected to be valuable for formulation and process development. During long processing times, the difference in the adhesion propensity of the two polyols may become critical and affect the feeding performance resulting in spikes of material being dislodged from the feeder outlet. Long-term investigations should therefore be performed to assess such risk. Additionally, CDC full line runs should be performed with different API formulations to evaluate the overall performance of the two polyols allowing a more thorough excipient profiling across the different unit operations and formulation cases. To enhance the fundamental understanding of the presented findings, the pre-blend feeding investigations would require a more detailed characterization of the blend structure. The latter will be in fact directly related to the fraction of particles dominating the type of contact interactions during tribo-charging.

Conclusions

In this study, we profiled the feeding performance and tribo-charging of P200SD and G721 powders. During split-feeding, G721 showed comparable feeding performance to the well-established P200SD, yet, with lower tribo-charging propensity and less tendency to adhere to the screw outlet. These observations were attributed to differences in inner structure, surface energy, and the presumed deformation characteristics of the powders. Compared to G721, P200SD was found to exhibit a highly porous structure with higher surface heterogeneity, larger surface area, and less surface water. All these factors may contribute to the overall higher charging tendency of P200SD.

The feeding performance of G721 was maintained during pre-blend feeding with minimal tribo-charging and adhesion tendency. The volumetric feeding capacity of P200SD was also consistent between split- and pre-blend feeding, whereas in the latter the adhesion propensity was reduced with the addition of 1 wt% of fine tracer powder. This was assumed to be due to a particle size-induced mitigation effect of powder electrostatics.

Overall, the results presented in this study evidenced the benefit of using G721 in continuous feeding operations when fed as single excipient as well as the possibility to mitigate the adhesion tendency of P200D in pre-blend formulations. Both aspects are deemed relevant for formulation and process development.

Supplementary Information The online version contains supplementary material available at https://doi.org/10.1208/s12249-023-02552-5.

Acknowledgements The authors would like to thank Patrick Gruber, Feroz Bhuiyan, and Paul Rinner for their support in the experimental work.

Author Contribution Michela Beretta: conceptualization, writing—original draft preparation, data curation. Julia Kruisz: formal analysis. Theresa R. Hörmann-Kincses: writing—review and editing. Viktoria Magosi: investigation. Meishan Guo: investigation. Majid Naderi: investigation. Sarah Heupl: investigation. Johann Kastner: investigation. Martin Spoerk: writing—review and editing. Amrit Paudel: conceptualization, supervision, writing—review and editing.

Funding Open access funding provided by Graz University of Technology. The Research Center Pharmaceutical Engineering (RCPE) is funded within the framework of COMET (Competence Centers for Excellent Technologies) by BMK, BMDW, Land Steiermark, and SFG. The COMET program is managed by the FFG.

Declarations

Conflict of Interest The authors declare no competing interests.

References

1. Bolhuis GK, Rexwinkel EG, Zuurman K. Polyols as filler-binders for disintegrating tablets prepared by direct compaction. Drug Dev Ind Pharm. 2009;35(6):671–7.
2. Ohrem HL, Schornick E, Kalivoda A, Ognibene R. Why is mannitol becoming more and more popular as a pharmaceutical excipient in solid dosage forms? Pharm Dev Technol. 2014;19(3):257–62.
3. Bolhuis GK, Engelhart JJP, Eissens AC. Compaction properties of isomalt. Eur J Pharm Biopharm. 2009;72:621–5.
4. Zarbock SD, Magnuson B, Hoskins L, Record KE, Smith KM. Lactose: The hidden culprit in medication intolerance? Orthopedics. 2007;30(8):615–7.
5. Bharate SS, Bharate SB, Bajaj AN. Interactions and incompatibilities of pharmaceutical excipients with active pharmaceutical ingredients: a comprehensive review. J Excipients Food Chem. 2010;1(3):3–26.
6. Karttunen A-P, Poms J, Sacher S, Sparén A, Samblás CR, Fransson M, et al. Robustness of a continuous direct compression line against disturbances in feeding. Int J Pharm. 2020;574: 118882.
7. Lakio S, Ervasti T, Tajarobi P, Wikström H, Fransson M, Karttunen A-P, et al. Provoking an end-to-end continuous direct compression line with raw materials prone to segregation. Eur J Pharm Sci. 2017;109:514–24.
8. Karttunen A, Wikström H, Tajarobi P, Fransson M, Sparén A, Marucci M, et al. Comparison between integrated continuous direct compression line and batch processing – the effect of raw material properties. Eur J Pharm Sci. 2019;133:40–53.
9. Rescaglio A, De Smet F, Aerts L, Lumay G. Tribo-electrification of pharmaceutical powder blends. Part Sci Technol. 2019;1–8
10. Barrios-Vazquez SC, Villafuerte-Robles L. Functionality of galenIQ 721 as excipient for direct compression tablets. J Appl Pharm Sci. 2013;3(4):8–19.
11. Muzíková J, Pavlasová V. Energy evaluation of the compaction process of directly compressible isomalt. Ces Slov Farm. 2011;60(1):11–6.
12. Govedarica B, Ilić I, Šibanc R, Dreu R, Srčič S. The use of single particle mechanical properties for predicting the compressibility of pharmaceutical materials. Powder Technol. 2012;225:43–51.
13. Rowe RC, Sheskey PJ, Quinn ME. Handbook of pharmaceutical excipients. 6th editio. Pharmaceutical Press; 2009
14. Mukherjee R, Sansare S, Nagarajan V, Chaudhuri B. Discrete element modeling (DEM) based investigation of tribocharging in the pharmaceutical powders during hopper discharge. Int J Pharm. 2021;596: 120284.
15. Engisch WE, Muzzio FJ. Loss-in-weight feeding trials case study: pharmaceutical formulation. J Pharm Innov. 2014;10:56–75.
16. Gold G, Palermo BT. Hopper flow electrostatics of tableting material I Instrumentation and acetaminophen formulations. J Pharm Sci. 1965;54(2):310–2.
17. Muehlenfeld C, Thommes M. Small-scale twin-screw extrusion - evaluation of continuous split feeding. J Pharm Pharmacol. 2014;66:1667–76.
18. Hsiao WK, Hörmann TR, Toson P, Paudel A, Ghiotti P, Stauffer F, et al. Feeding of particle-based materials in continuous solid dosage manufacturing: a material science perspective. Drug Discov Today. 2020;25(4):800–6.
19. Bostijn N, Dhondt J, Ryckaert A, Szabó E, Dhondt W, Van Snick B, et al. A multivariate approach to predict the volumetric and gravimetric feeding behavior of a low feed rate feeder based on raw material properties. Int J Pharm. 2019;557:342–53.
20. Stauffer F, Vanhoorne V, Pilcer G, Chavez PF, Schubert MA, Vervaet C, et al. Managing active pharmaceutical ingredient raw material variability during twin-screw blend feeding. Eur J Pharm Biopharm. 2019;135:49–60.
21. Bekaert B, Penne L, Grymonpre W, Van Snick B, Dhondt J, Boeckx J, et al. 2021 Determination of a quantitative relationship between material properties, process settings and screw feeding behavior via multivariate data-analysis. Int J Pharm. 602(120603)
22. Beretta M, Hörmann TR, Hainz P, Hsiao W-K, Paudel A 2020 Investigation into powder tribo-charging of pharmaceuticals. Part I: process-induced charge via twin-screw feeding. Int J Pharm. 591(120014)

23. Allenspach C, Timmins P, Lumay G, Holman J, Minko T. Loss-in-weight feeding, powder flow and electrostatic evaluation for direct compression hydroxypropyl methylcellulose (HPMC) to support continuous manufacturing. Int J Pharm. 2021;596: 120259.
24. Karner S, Urbanetz NA. Arising of electrostatic charge in the mixing process and its influencing factors. Powder Technol. 2012;226:261–8.
25. Pu YU, Mazumder M, Cooney C. Effects of electrostatic charging on pharmaceutical powder blending homogeneity. J Pharm Sci. 2009;98:2412–21.
26. Naik S, Mukherjee R, Chaudhuri B. Triboelectrification: a review of experimental and mechanistic modeling approaches with a special focus on pharmaceutical powders. Int J Pharm. 2016;510:375–85.
27. Kaialy W. A review of factors affecting electrostatic charging of pharmaceuticals and adhesive mixtures for inhalation. Int J Pharm. 2016;503:262–76.
28. Beretta M, Hörmann TR, Hainz P, Hsiao WK, Paudel A. Investigation into powder tribo–charging of pharmaceuticals. Part II: Sensitivity to relative humidity. Int J Pharm. 2020;591(120015)
29. Paul S, Chang SY, Dun J, Sun WJ, Wang K, Tajarobi P, et al. Comparative analyses of flow and compaction properties of diverse mannitol and lactose grades. Int J Pharm. 2018;546:39–49.
30. Greenspan L. Humidity fixed points of binary saturated aqueous solutions. J Res Natl Bur Stand - A Phys Chem. 1977;81(1):89–96.
31 Hörmann-Kincses TR, Beretta M, Kruisz J, Stauffer F, Birk G, Piccione PM, et al. Predicting powder feedability: a workflow for assessing the risk of flow stagnation and defining the operating space for different powder-feeder combinations. Int J Pharm. 2022;629(122364)
32. Li T, Scicolone JV, Sanchez E, Muzzio FJ. Identifying a loss-in-weight feeder design space based on performance and material properties. J Pharm Innov. 2020;15(3):482–95.
33. Wang Y, Li T, Muzzio FJ, Glasser BJ. Predicting feeder performance based on material flow properties. Powder Technol. 2017;308:135–48.
34. Kastner J, Heinzl C. X-ray tomography. In: Handbook of Advanced Non-Destructive Evaluation. Springer; 2018. p. 1–72.
35 Barrett EP, Joyner LG. Halenda PP The determination of volume and area distributions in porous substances I. Computations from nitrogen isotherms. J Am Chem Soc. 1951;73:373–80.
36. Washburn EW. The dynamics of capillary flow. Phys Rev. 1921;17(3):273–83.
37. Dorris GM, Gray DG. Adsorption of n-alkanes at zero surface coverage on cellulose paper and wood fibers. J Colloid Interface Sci. 1980;77(2):353–62.
38. Van Oss CJ, Chaudhury MK, Good RJ. Interfacial Lifshitz-van der Waals and polar interactions in macroscopic systems. Chem Rev. 1988;88:927–41.
39. Jallo LJ, Dave RN. Explaining electrostatic charging and flow of surface-modified acetaminophen powders as a function of relative humidity through surface energetics. J Pharm Sci. 2015;104(7):2225–32.
40. Santos O, Nylander T, Rosmaninho R, Rizzo G, Yiantsios S, Andritsos N, et al. Modified stainless steel surfaces targeted to reduce fouling - surface characterization. J Food Eng. 2004;64:63–79.
41. Santos B, Carmo F, Schlindwein W, Muirhead G, Rodrigues C, Cabral L, et al. Pharmaceutical excipients properties and screw feeder performance in continuous processing lines: a quality by design (QbD) approach. Drug Dev Ind Pharm. 2018;44:2089–97.
42. Vehring R. Pharmaceutical particle engineering via spray drying. Pharm Res. 2008;25(5):999–1022.
43. Carr RL. Evaluating Flow Properties of Solids. Chem Eng. 1965;72:163–8.
44. Li XH, Zhao LJ, Ruan KP, Feng Y, Xu DS, Ruan KF. The application of factor analysis to evaluate deforming behaviors of directly compressed powders. Powder Technol. 2013;247:47–54.
45. Sarkar S, Cho J, Chaudhuri B. Mechanisms of electrostatic charge reduction of granular media with additives on different surfaces. Chem Eng Process. 2012;62:168–75.
46. Mukherjee R, Gupta V, Naik S, Sarkar S, Sharma V, Peri P, et al. Effects of particle size on the triboelectrification phenomenon in pharmaceutical excipients: experiments and multi-scale modeling. Asian J Pharm Sci. 2016;11:603–17.
47 Zheng XJ, Huang N, Zhou YH. Laboratory measurement of electrification of wind-blown sands and simulation of its effect on sand saltation movement. J Geophys Res Atmos. 2003;108(D10):4322.
48. Samiei L, Kelly K, Taylor L, Forbes B, Collins E, Rowland M. The influence of electrostatic properties on the punch sticking propensity of pharmaceutical blends. Powder Technol. 2017;305:509–17.
49. Zhou H, Götzinger M, Peukert W. The influence of particle charge and roughness on particle-substrate adhesion. Powder Technol. 2003;135–136:82–91.
50. Bunker MJ, Davies MC, James MB, Roberts CJ. Direct observation of single particle electrostatic charging by atomic force microscopy. Pharm Res. 2007;24(6):1165–9.
51. McCarty LS, Whitesides GM. Electrostatic charging due to separation of ions at interfaces: contact electrification of ionic electrets. Angew Chem Int Ed. 2008;47:2188–207.
52. Alan BO, Barisik M, Ozcelik HG. Roughness effects on the surface charge properties of silica nanoparticles. J Phys Chem C. 2020;124(13):7274–86.
53. Schella A, Herminghaus S, Schröter M. Influence of humidity on tribo-electric charging and segregation in shaken granular media. Soft Matter. 2017;13:394–401.
54. Zellnitz S, Pinto JT, Brunsteiner M, Schroettner H, Khinast J, Paudel A. Tribo-charging behaviour of inhalable mannitol blends with salbutamol sulphate. Pharm Res. 2019;36:80.
55. Pinto JT, Wutscher T, Stankovic-Brandl M, Zellnitz S, Biserni S, Mercandelli A, et al. Evaluation of the physico-mechanical properties and electrostatic charging behavior of different capsule types for inhalation under distinct environmental conditions. AAPS PharmSciTech. 2020;21(128)
56. Forward KM, Lacks DJ, Sankaran RM. Charge segregation depends on particle size in triboelectrically charged granular materials. Phys Rev Lett. 2009;102:028001
57 Waitukaitis SR, Lee V, Pierson JM, Forman SL, Jaeger HM. Size-dependent same-material tribocharging in insulating grains. Phys Rev Lett. 2014;112(218001)